Different inhibition of Nrf2 by two Keap1 isoforms α and β to shape malignant behaviour of human hepatocellular carcinoma

Feilong Chen[1],Mei Xiao[1], Jing Feng[1], Reziyamu Wufur[1,2] ,Keli Liu[1] ,Shaofan Hu [1,2] , Guiyin Sun [2]*, and Yiguo Zhang [1,2]*
1 The Laboratory of Cell Biochemistry and Topogenetic Regulation, College of Bioengineering and Faculty of Medical Sciences, Chongqing University, No. 174 Shazheng Street, Shapingba District, Chongqing 400044, China
2 Chongqing University Jiangjin Hospital, School of Medicine, Chongqing University, No. 725 Jiangzhou Avenue, Dingshan Street, Jiangjin District, Chongqing 402260, China
*Correspondence to YZ: yiguozhang@cqu.edu.cn; or GS: sunriseok@126.com

Abstract:

Nrf2 plays a crucial role in the management of oxidative and electrophilic stress. Nrf2 acts as a master regulator of oxidative or metabolic stress responses and is involved in cancer cell metabolism and multiple oncogenic pathways. Keap1 is the main inhibitor of Nrf2, and its high or low expression also causes changes in Nrf2. The function of Keap1 isoforms has rarely been reported. Here, to gain a better understanding of their similarities and differences in distinct regulatory profiles, four distinct cell models stably expressing *Keap1*$^{-/-}$, *Keap1β (Keap1*$^{\Delta 1\text{-}31}$*)*, *Keap1-Restored* or *Keap1α-Restored* have been established. Immunofluorescence localization and nucleocytoplasmic separation experiments found that Keap1 and its isoforms were localized in the cytoplasm and had inhibitory effects on Nrf2 and HO-1. Further transcriptome analysis revealed that they had similar and different functions. Their functions were further explored in vivo (subcutaneous tumour formation in nude mice) and in vitro (cell cloning, infection, migration, wound healing, CAT, GSH, cell cycle and apoptosis). Next, the results of tumorigenesis experiments in nude mice were verified based on changes in the PTEN and PI3K-mTOR pathways. Finally, some typical genes of EMT, cell cycle and apoptosis were detected, and the experimental results were verified by in vitro experiments.

Keywords: Keap1, Keap1α, Keap1β, Nrf2, PTEN, PI3K-mTOR pathway, EMT,

1. Introduction

Keap1 was originally isolated by a yeast two-hybrid system[1]. The full-length Keap1 protein is composed of 624 amino acids (aa) with a molecular weight of 69 kDa[2] and contains six exons and five introns located on chromosome 19p13.2[3]. Nevertheless, there have been few reports on its protein isoforms. The functions of Keap1 protein isoforms (Keap1a and Keap1b) have been reported in zebrafish[4], and a novel natural mutant of Keap1 (Keap1$^{\Delta C}$) was also reported, which lacked most of its C-terminal key Nrf2-interacting domain (b-ZIP) that inhibits the leucine zipper of the cap 'n' collar (CNC) base-region factor[3]. In addition, Keap1 has been identified as a master inhibitor of Nrf2 (nuclear factor-erythroid 2-related factor 2), and high or low expression of Keap1 in human lung, breast, liver and other somatic cancers also causes changes in Nrf2[5,6].

As one of the most important members of the CNC-bZIP family[7,8], Nrf2 plays a crucial role in the management of oxidative and electrophilic stress. Nrf2 originated in foreign organisms as a master regulator in response to oxidative or metabolic stress and has been implicated in metabolism as well as multiple oncogenic pathways in cancer cells[9]. Further studies have demonstrated the physiological importance of Nrf2-dependent cytoprotection in Nrf2-deficient mice[10], rats[11] and zebrafish[12]. The unstimulated Nrf2 protein remained in the cytoplasm and directly bound to Keap1[13,14]. Keap1 promoted Nrf2 protein degradation through the ubiquitin–proteasome system of Cullin3[15,16]. After

Nrf2 is activated, it is separated from Keap1[17]. Activated Nrf2 is translated into the nucleus and bound to antioxidant response elements (AREs) and small MAF transcription factors[15]. A large number of Nrf2-dependent antioxidant genes and detoxification enzymes are transcriptionally activated and expressed, including HO-1 (haeme oxygenase 1), GSR (glutathione reductase), NQO1 (NAD(P)H quinone oxidoreductase-1), GCLC (γ-glutamyl cysteine ligase catalytic subunit), and GCLM (γ-glutamate-cysteine ligase modifier subunit), among others[15,17].

Herein, we found that Keap1 has two main isoforms, which are formed by different transcriptional translations and differentially expressed in different cells and tissues. For descriptive convenience, we name them Keap1α (larger molecular weight) and Keap1β (smaller molecular weight). To explore the functional differences between Keap1α and Keap1β, we constructed Keap1$^{-/-}$ and *Keap1β (Keap1$^{\Delta 1\text{-}31}$)* cell lines, and the stable expression of Keap1 and Keap1α was restored by the lentiviral system using the Keap1$^{-/-}$ cell line. When Keap1 is knocked out, cell proliferation and migration of tumour xenografts are reduced. However, this effect was reversed to varying degrees when Keap1, Keap1α and Keap1β were restored in Keap1$^{-/-}$ cells. A series of comparative experiments (subcutaneous tumour formation in nude mice, cell cloning, infection, migration, CAT, GSH, wound healing, EMT, cell cycle progression and apoptosis) were used to verify the similarities and differences in their regulatory functions. Further transcriptome sequencing analysis revealed that Keap1α and Keap1β are involved in distinct signalling pathways.

2. MATERIALS AND METHODS

2.1. Cells, Cell Culture and Transfection

The *HepG2* cells used in this study were purchased from the Cell Bank of Type Culture Collection of Chinese Academy of Sciences (Shanghai, China). *Keap1$^{-/-}$* and *Keap1β(Keap1$^{\Delta 1\text{-}31}$)* cells were created by CRISPR/Cas9 technology. *Keap1-Restored* and *Keap1α-Restored* cells were created by stably expressing related proteins using lentivirus technology. They were trained according to the relevant requirements. Transfection was performed using the Lipofectamine 3000 Transfection Kit (Invitrogen), which can transfect one or more plasmids. Transfection experiments were performed according to the kit instructions.

2.2. Chemicals and Antibodies

All chemicals were of the best quality commercially available. The protein primary antibody to Nrf1 (NFE2L1) was derived from our own experiments. DYKDDDDK Tag Monoclonal Antibody (FG4R) was purchased from Invitrogen, and other primary antibodies were derived from Abcam. Secondary antibodies and β-actin were purchased from ZSGB-BIO (Beijing, China).

2.3. Expression Constructs

The human full-length Keap1 and Nrf2 cDNA sequences were subcloned into a pcDNA3 or 3XFlag vector, respectively. The Keap1α plasmid was obtained by mutating the 2nd ATG (32nd amino acid) from the N-terminus in the Keap1 full-length plasmid. The first 31 amino acids (the first 93 bases) of the N-terminus were mutated in the full-length Keap1 plasmid to obtain the Keap1β plasmid.

2.4. Stable Expression of the *Keap1$^{-/-}$*, *Keepβ(Keap1$^{\Delta 1\text{-}31}$)*, *Keap1-Restored* and *Keap1α-Restored* Constructs

In *HepG2* cells, CRISPR/Cas9 gene editing technology was used for gene knockout, and *Keap1$^{-/-}$* and

Keap1β(Keap1$^{\Delta 1-31}$) cells were constructed and identified by sequencing (Figure S1A-D). The full-length cDNA sequences of the Keap1 and Keap1α plasmids were cloned into the pLVX-IRES-ZsGreen-puro vector for lentivirus packaging. We made lentiviruses according to previous methods[18]. *Keap1$^{-/-}$* cells were infected with Keap1 and Keap1α lentiviral plasmids, and stably expressing cells (*Keap1-Restored* and *Keap1α-Restored*) were constructed and identified by quantitative real-time PCR (q-PCR) and Western blotting (WB) experiments (Figure 1C). Experimental cell lines were screened with puromycin.

2.5. RNA Isolation and Quantitative Real-Time PCR (qPCR)

Total RNA was prepared from cells using the RNA Simple Total RNA Kit (DP419, Tiangen Biotech Co., Ltd., Beijing, China), and reverse transcription was performed using the Revert Aid First Strand cDNA Synthesis Kit from Thermo.

2.6. Nucleocytoplasmic Separation Analysis

Experimental cells (4.0×10^5) were grown on 6-cm cell culture plates for 48 h. A nucleocytoplasmic separation kit was purchased from Sigma (N-3408-200ML). Nucleocytoplasmic separation experiments were performed according to the kit instructions.

2.7. Transwell Analysis

Transwell assays were performed in modified Boyden chambers (8 µm, 24-well insert; Transwell; Corning Inc. Lowell, MA, USA). Briefly, after the growing cells reached 75%-85% confluency, they were starved in serum-free medium for 12 h. Medium containing foetal bovine serum was added to the lower chamber, and experimental cells (5,000 or 5.0×10^3) in 500 µL of serum-free medium were added to the upper chamber. Cells were cultured at 37 °C for 24 h. The cells were fixed with precooled paraformaldehyde fixative (Serbicebio) for 30 minutes and stained with crystal violet (Beyotime) for 30 minutes at room temperature. All the above operations required three washes with PBS, and cells were photographed and counted.

2.8. Colony-formation Analysis

Equal numbers (1,000 or 1×10^3) of experimental cells (*Keap1$^{+/+}$*, *Keap1$^{-/-}$*, *Keap1-Restored*, *Keap1α-Restored* and *Keap1β(Keap1$^{\Delta 1-31}$)*) were allowed to grow for 10 days. The same experiment was repeated 3 times. The colonies were fixed with precooled paraformaldehyde fixative (Serbicebio) for 30 minutes and stained with crystal violet (Beyotime) for 30 minutes at room temperature. All the above operations required three washes with PBS, and cells were photographed and counted.

2.9. Wound-healing Analysis

When experimental cells (4.0×10^5) were grown in 6-well plates to 80-85% confluency, they were starved in serum-free medium for 12 hours. Experimental cells were wounded with a 20-µL pipette tip and washed with PBS. The distance of cell removal was observed by microscopy at different time points (0, 24, 48 and 72 h).

2.10. CAT and GSH Level Analyses

Experimental cells (4.0×10^5) were grown on 6-cm cell culture plates for 24 h. After the cells were digested, they were collected into 1.5 ml centrifuge tubes. The CAT (catalase) activity detection kit was purchased from Solarbio (BC0205), and the GSH (reduced glutathione) assay kit was purchased from

Nanjing Jiancheng Bioengineering Institute (A006-2-1). CAT and GSH levels were determined according to the kit instructions. The above experiments were repeated 3 times.

2.11. Cell Cycle and Apoptosis Detection by Flow Cytometry

Experimental cells (4.0×10^5) were grown on 6-cm cell culture plates for 24 h. Afterwards, the cells were starved in serum-free medium for 12 h before being treated with 10 µmol/L BrdU for 12 h. The cells were fixed for 15 min with 100 µl of BD Cytofix/Cytoperm buffer (containing a mixture of paraformaldehyde as a fixative and saponin as a detergent) at room temperature and permeabilized for 10 min with 100 µl of BD Cytoperm permeabilization buffer plus (containing foetal bovine serum as a staining enhancer) on ice. Thereafter, the cells were refixed and treated with 100 ml DNase (at a dose of 300 mg/ml in DPBS) for 60 min at 37 °C to expose the incorporated BrdU, followed by staining with FITC-conjugated anti-BrdU antibody for 1 h at room temperature. Subsequently, the cells were suspended in 20 ml of 7-amino-actinomycin D solution for 20 min for DNA staining and resuspended in 0.5 ml of staining buffer (i.e., 1× DPBS containing 0.09% sodium azide and 3% heat-inactivated FBS) prior to cell cycle analysis by flow cytometry. Furthermore, cells (6×10^5) were allowed to grow for 48 h in 6-cm dishes before being harvested for apoptosis analysis. The cells were pelleted by centrifuging at 500×g for 5 min and washed with PBS 3 times before being incubated for 15 min with 5 ml of Annexin V-FITC and 10 ml of propidium iodide (PI) in 195 ml of binding buffer, followed by apoptosis analysis by flow cytometry. These results were obtained using a low flow rate of 400 events per second and were further analysed by FlowJo 7.6.1 software[19].

2.12. Western Blotting Analysis (WB)

Experimental cells were washed 3 times with PBS, and total cell protein was extracted using the total protein extract. At 100 °C, the total protein lysate was immediately denatured for 10 minutes. The eluted proteins were separated by SDS–PAGE at different concentrations (8, 10 and 15%). Different primary antibodies (Keap1, Nrf2, HO-1 and PTEN, etc.) and secondary antibodies (mouse and rabbit) were used for WB.

2.13. Coimmunoprecipitation (Co-IP) and immunoblot analyses

HepG2 cells (4.0×10^5) were grown on 6-well cell culture plates for 24 h. Different plasmids (Keap1-Flag, Keap1α-Flag, Keap1β-Flag and Nrf2-V5) were transfected into HepG2 cells. After 8 h of transfection, the normal medium was replaced for 24 h. The experimental cells were lysed in RIPA buffer (C1053, PPLYGEN) containing protease and phosphatase inhibitors (Solarbio, P6730). Cell lysates were centrifuged, and the resulting supernatants were subjected to coimmunoprecipitation with antibodies against V5 or Flag using BeyoMag™ Protein A+G beads (Beyotime [20], P2108-1ML). The eluted proteins were separated by SDS–PAGE. The membranes were probed with anti-V5 antibody (Invitrogen) and anti-Flag (Invitrogen) antibody and then with horseradish peroxidase-conjugated secondary antibodies (ZSGB-BIO, ZB-2305, 0.1ML) and enhanced chemiluminescence reagents (Thermo, iBright 750[21]).

2.14. Immunofluorescence and confocal microscopy

Alcohol-soaked glass coverslips were stored flat in six-well plates. Cos-1 cells (2.5×10^5) were grown on 6-well cell culture plates for 24 h. Different plasmids (Keap1-V5, Keap1α-V5 and Keap1β-V5) were transfected into Cos1 cells. Experimental cells were plated onto 1 cm^2 coverslips (for analyses using a fluorescence microscope). After transfection for 8 h and culture for 24 h, the cells were washed in

phosphate-buffered saline (PBS) and fixed with paraformaldehyde fixative (Servicebio, Wuhan) for 30 min at room temperature. The experiments were conducted at room temperature. Cells were then rinsed 3 times with PBS and permeabilized with 0.2% Triton X-100 for 20 min. Cells were then rinsed 3 times with PBS and permeabilized with 1% BSA for 60 min. The primary antibody was incubated overnight, and the secondary Alexa Fluor–conjugated secondary antibody (anti-mouse or anti-rabbit antibody, ZSGB-BIO) was incubated for 4 hours. The cells were incubated with a flag-tagged primary antibody against endogenous actin, and the previous step was repeated. The cells were then rinsed 3 times with PBS, and the coverslips were mounted with DAPI (Beyotime, C1005). Plates were imaged using an IN Cell Analyzer Zeiss LSM900 cellular imaging system[22].

2.15. Transcriptome sequencing analysis

Total RNA was extracted from experimental cells using an RNAsimple total RNA Kit. Beijing Genomics Institute (BGI, Shenzhen, China) was responsible for sequencing the transcriptome data on an Illumina HiSeq 2000 sequencing system (Illumina, San Diego, CA). All differentially expressed genes (DEGs) were identified, and the standard fold change was ≥2 or ≤0.5, with an FDR (false discovery rate) of ≤0.001 by the Poisson distribution model method (PossionDis). These data were analysed according to a previous method[18,23].

2.16. Subcutaneous Tumour Xenografts in Nude Mice

All relevant animal experiments complied with the regulations of the Animal Ethics Committee in this study. All mice were kept under the conditions of an SPF experimental animal room. We conducted two subcutaneous tumour experiments in mice. In the first experiment, mouse xenograft models were made by subcutaneous heterotransplantation of wild-type *HepG2* (*Keap1*$^{+/+}$), *Keap1*$^{-/-}$, *Keap1β(Keap1*$^{\Delta 1-31}$*)* cells into nude mice as described[24]. In the second experiment, mouse xenograft models were made by subcutaneous heterotransplantation of *Keap1*$^{-/-}$, *Keap1-Restored* and *Keap1α-Restored* cells into nude mice as described[24]. The experimental cells (1.0×10^7) in the exponential growth phase were digested and suspended in 0.1 ml of PBS and then subcutaneously inoculated into male nude mice (BALB/cnu/nu, 6 weeks, 15 g, 6 mice per group, from HFK Bioscience, Beijing, China) at a single point in the back area. The sizes of the tumours were measured every other day.

In the first experiment, the mice were sacrificed on the 24th day, and their transplanted tumours were excised. In the second experiment, the mice were sacrificed on the 30th day, and their transplanted tumours were excised. The sizes of growing tumours were calculated by a standard formula: $V = a\,(\text{length}) \times b^2\,(\text{width}^2)/2$.

2.17. HE Staining and Immunohistochemistry

Subcutaneous tumours of nude mice were treated with paraformaldehyde fixative (Servicebio, Wuhan) for 24 h. The tumour tissues were subjected to histopathological examination (HE) by routine haematoxylin-eosin staining, followed by immunohistochemical staining with antibodies against Keap1 and PTEN. The histopathological examination staining and immunohistochemical antibodies were provided by Servicebio.

2.18. Statistical Analysis

The statistical significances of cell proliferation, migration, cycle, apoptosis, invasion and gene expression were determined using either Student's t test (for comparisons between two groups) or

two-way ANOVA (for comparisons among multiple groups). The relevant data are shown as fold changes (mean ± SEM or ± SD) with significant differences that were calculated by the value of $p < 0.05$.

3. Results

3.1. Four cells with stable expression of *Keap1*$^{-/-}$, *Keap1β(Keap1*$^{\Delta 1-31}$*)*), *Keap1-Restored*, and *Keap1α-Restored* were established.

First, we constructed the Keap1$^{-/-}$ cell line using Cas9 technology. The results of qPCR and western blotting showed that Keap1 was no longer expressed in *Keap1*$^{-/-}$ cells (Figure 1A), and sequencing of their genomic DNA showed that both alleles of Keap1 dropped 10 bases, which resulted in a change in the reading frame of Keap1 (Figure S1A, B). In this process, we obtained another cell line expressing only the smaller band of Keap1, which we named Keap1b (Figure 1B). Further sequencing revealed a base insertion before the 23rd base in the CDS region of Keap1 (Figure S1C, D). We therefore speculated that this base insertion resulted in a change in the reading frame that expressed the larger band of Keap1, and we named the larger band Keap1α.

To verify this hypothesis, we made a full-length sequence plasmid of pLVX-mcmv-ZsGreen-puro pKeap1. Through data alignment on the NCBI website, we found that the second N-terminal promoter ATG of Keap1 is the 32nd amino acid. It is possible that the 32nd amino acid is critical for Keap1β expression. By mutating the plasmid, the 32nd amino acid (the second ATG) was deleted to create pLVX-mcmv-ZsGreen-puro pKeap1α. Through lentivirus infection, two cell lines (*Keap1-Restored* and *Keap1α-Restored*) were constructed in Keap1$^{-/-}$ cells, and the resulting *Keap1-Restored* and *Keap1α-Restored* cells were confirmed by q-PCR and WB (Figure 1C). The experimental results also showed that amino acid 32 determines the expression of Keap1β. Therefore, the expression of Keap1 and its isoforms (α and β) was caused by the differential expression of amino acids, and the key points were the first and 32nd amino acids (Figure 1D). When the 32nd amino acid was deleted from the N-terminus, only Keap1α was expressed, and when amino acids 1-31 were deleted from the N-terminus, only Keap1β was expressed.

Keap1 is an inhibitor of Nrf2, a transcription factor involved in oxidative stress responses. The Keap1-Nrf2 pathway is an important redox pathway. Compared with *Keap1*$^{+/+}$, the expression levels of *Nrf2* and *HO-1* were increased in *Keap1*$^{-/-}$ cells, but they were decreased in *Keap1β(Keap1*$^{\Delta 1-31}$*)* cells (Figure 1E). Compared with *Keap1*$^{-/-}$, in *Keap1-Restored* and *Keap1α-Restored* cells, the expression levels of both *Nrf2* and *HO-1* were reduced, but the decrease in *Keap1-Restored cells* was more obvious (Figure 1F). The cytoskeleton protein actin was used for immunofluorescence experiments, and the results showed that Keap1, Keap1α and Keap1β were all located in the cytoplasm (Figure 1G). Reciprocal immunoprecipitation assays revealed that Nrf2 interacted with Keap1, Keap1α and Keap1β (Figure 1H). Through nucleocytoplasmic separation experiments, we found that in the absence of Keap1, Nrf2 and HO-1 were upregulated in the cytoplasm, while overexpression of Keap1β resulted in significant downregulation (Figure 1I). The results also showed that when Keap1 (*Keap1α-Restored* cells) and Keap1α (*Keap1α-Restored* cells) were overexpressed, Nrf2 and HO-1 were significantly downregulated in the nucleus and cytoplasm (Figure 1J). Overall, both Keap1α and Keap1b can bind and regulate Nrf2, but to different degrees.

Figure 1

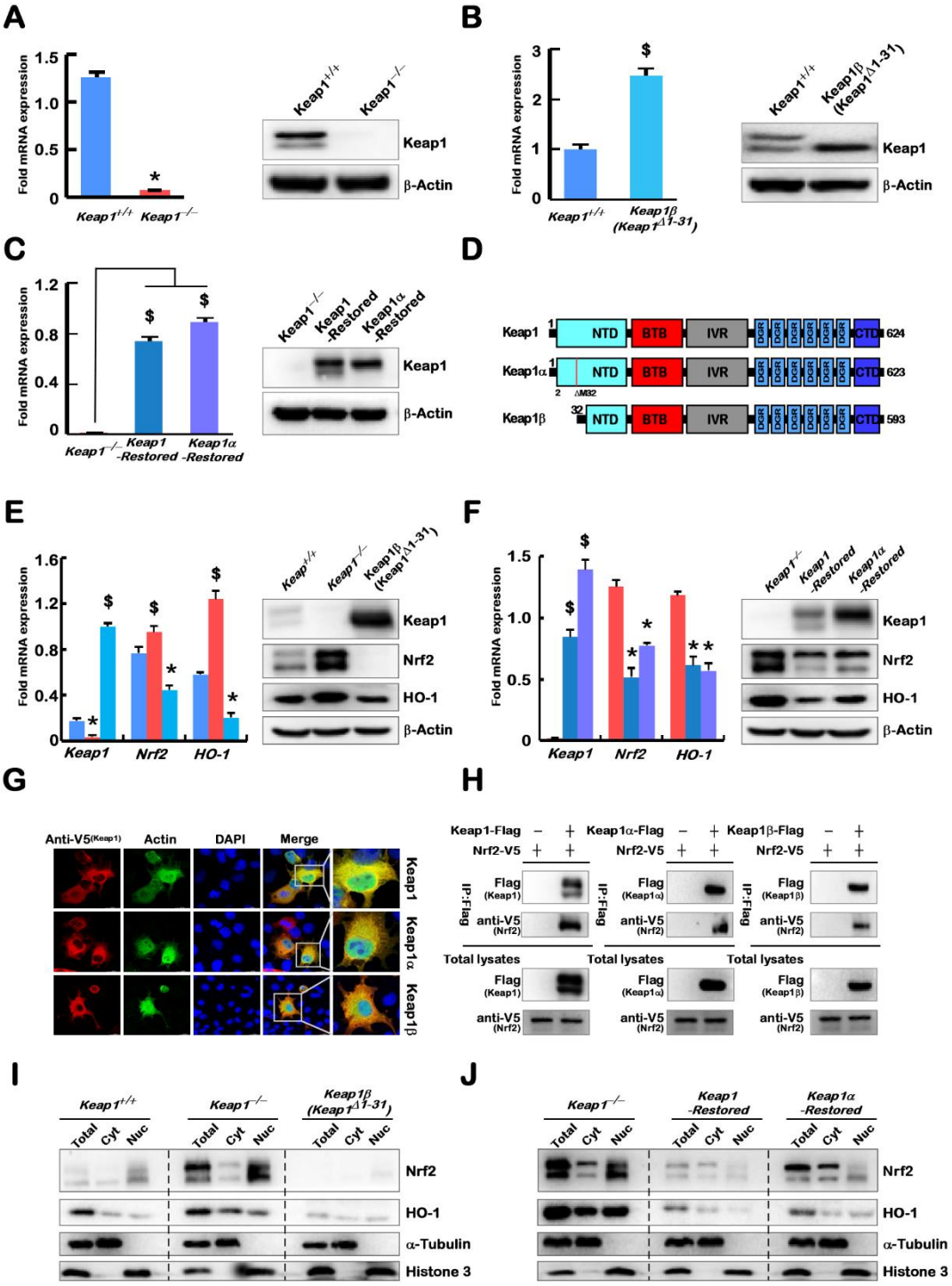

Figure 1. Construction of cells, function and localization of Keap1 and its isoform (α and β). **(A-C)** Identification of *Keap1*$^{-/-}$**(A)**, *Keap1β(Keap1*$^{\Delta 1\text{-}31}$*)* **(B)**, *Keap1-Restored***(C)** and *Keap1α-Restored***(C)** cells by q-PCR and WB. **(D)**Protein sequence cartoon. Compared with Keap1, Keap1α lacks the 2nd promoter (ATG) or the 32nd amino acid, Keap1β lacks the first 31 amino acids. **(E)** The expression levels (mRNA and protein) of *Keap1*, *Nrf2*, and *HO-1* in *Keap1*$^{+/+}$, *Keap1*$^{-/-}$ and *Keap1β(Keap1*$^{\Delta 1\text{-}31}$*)* cells were compared by q-PCR and WB. **(F)** The expression levels (mRNA and protein) of *Keap1*, *Nrf2*, and *HO-1* in *Keap1*$^{-/-}$, *Keap1-Restored* and *Keap1α-Restored* cells were compared by q-PCR and WB. **(G)** Subcellular localization of Keap1 and its isoforms (α and β). Cos1 cells were transfected with Keap1-V5, Keap1α-V5 or Keap1β-V5 plasmids, respectively, incubated with primary antibody and fluorescent secondary antibody, and stained with DAPI. Incubate with a flag-tagged primary antibody against endogenous Actin. The fluorescence intensity of protein was measured and observed by immunofluorescence microscope. Pictures showed representative examples. Scale bars, 20 μm. **(H)** Binding of Nrf2 to Keap1 and its isoforms (α and β) was verified by co-

immunoprecipitation (CO-IP) method. Cos1 cells were transfected with Nrf2 and Keap1, Keap1α or Keap1β plasmids, respectively. After 8 h of transfection, the normal medium was replaced for 24 h, and the total protein was collected. Immunoprecipitates and total cell lysates were analyzed by immunoblotting as indicated. **(I, J)** Localization of Nrf2 inhibition by Keap1 and its isoforms (α and β). According to the operating steps of the kit, the cytoplasm and nucleus were extracted from the five cell lines. Western blot (WB)was used to detect the protein expressions of Nrf2, H0-1 and α-Tubulin and Histone3.N≥3, and "*" "$" indicates p≤0.01.

3.2. Differential expression profiles of genes regulated by *Keap1*$^{-/-}$, *Keap1-Restored*, *Keap1α-Restored* and *Keap1β (Keap1*$^{\Delta 1\text{-}31}$*)* were defined.

To identify differential expression profiles of genes regulated by *Keap1*$^{-/-}$, Keap1-Restored, *Keap1α-Restored* and *Keap1β(Keap1*$^{\Delta 1\text{-}31}$*)*, transcriptome sequencing was used to analyse relevant RNAs extracted from established model cells. Therefore, all of these detectable genes, those up- or downregulated with fold changes ≥2 or ≤0.5 plus a false discovery rate (FDR) ≤0.001 (Figure 2A), were defined as differentially expressed genes (DEGs) by comparison with control cells (Keap1$^{+/+}$ cells) under the same conditions. As a result, 1147 DEGs were detected in *Keap1*$^{-/-}$ cells, including 756 target genes upregulated and 391 target genes downregulated (Figure 2A and Table S1). Notably, 887 DEGs were identified in *Keap1-Restored* cells, of which 640 were upregulated and 247 were downregulated (Table S2). In contrast, *Keap1α-Restored* cells resulted in 640 upregulated and 247 downregulated genes (Table S3), whereas Keap1β(Keap1$^{\triangle 1\text{-}31}$) cells led to a significantly decreased number of upregulated genes (i.e., 235) accompanied by the downregulation of 157 DEGs (Table S4). Together, these data indicate that their DEGs were significantly reduced when only isoforms (α or β) of Keap1 were expressed. The common genes between every two cell groups and every specific gene were screened (Figure 1B), and these comparison groups had distinct differences. Notably, genes regulated by Keap1 and its isoforms (α and β) were more likely to be upregulated than downregulated (Figure 1B and Table 3).

Furthermore, the biological process terms and pathways were classified by using the KEGG and QuickGO databases. Differentially expressed genes were used for KEGG pathway and GO enrichment analyses and screened for the top 10 functions for comparison (Figure S2). Such functional annotation analysis implied that DEGs regulated by Keap1 (*Keap1*$^{-/-}$ and *Keap1-Restored* cells) were predominantly involved in cancer, signal transduction, cellular community, infectious disease, signalling molecules and interaction, immune system process, metabolic process, biological adhesion, developmental process, cellular process, biological regulation and cellular process. Keap1α-regulated (*Keap1α-Restored* cells) DEGs were responsible for cancer, endocrine and metabolic disease, immune disease, immune system, substance dependence, cell growth and death, cardiovascular disease, infectious disease, signal transduction, immune system process, biological regulation, cellular process, developmental process, biological regulation, cellular process and biological regulation. Keap1β-regulated (*Keap1β(Keap1*$^{\Delta 1\text{-}31}$*)* cells) DEGs were also responsible for endocrine and metabolic disease, cardiovascular disease, cancer, signal transduction, signalling molecules and interaction, infectious disease, developmental process, cell proliferation, biological adhesion, developmental process, biological regulation, positive regulation of biological process, cellular process and biological regulation. From the above results, we found that they had highly related functions. According to Figure S2, the PI3K-AKT pathway was found multiple times in the KEGG pathway analysis.

The crossover of DEGs regulated by *Keap1*$^{-/-}$, *Keap1-Restored*, *Keap1α-Restored* and *Keap1β(Keap1*$^{\Delta 1\text{-}31}$*)* are displayed in a Venn diagram (Figure 2C). Their specific DEGs were as follows: 297 *Keap1*$^{-/-}$ cells, 68 *Keap1-Restored* cells, 143 *Keap1α-Restored* cells, and 166 *Keap1β(Keap1*$^{\Delta 1\text{-}31}$*)* cells. The top 10 KEGG pathways and GO enrichment functions of these specific DEGs were analysed in detail in another article from our group. Approximately 137 DEGs were screened to be shared among the four

cells, as shown in the Venn diagram (Figure 2C and Table S5). The differential expression levels of these common DEGs (137) were presented by differential clustering heatmaps (Figure 2D). These genes were also subjected to biological process analysis. Their biological processes mainly focus on cellular processes, metabolic processes, biological regulation, positive regulation of biological processes and responses to stimuli. Among the shared DEGs, only 36 genes showed inconsistent trends, and the remaining genes showed similar expression trends (both up- and downregulated) in all four cell lines (Figure 2D). Together, the functions of Keap1, Keap1α and Keap1β overlap greatly, but there are still some differences.

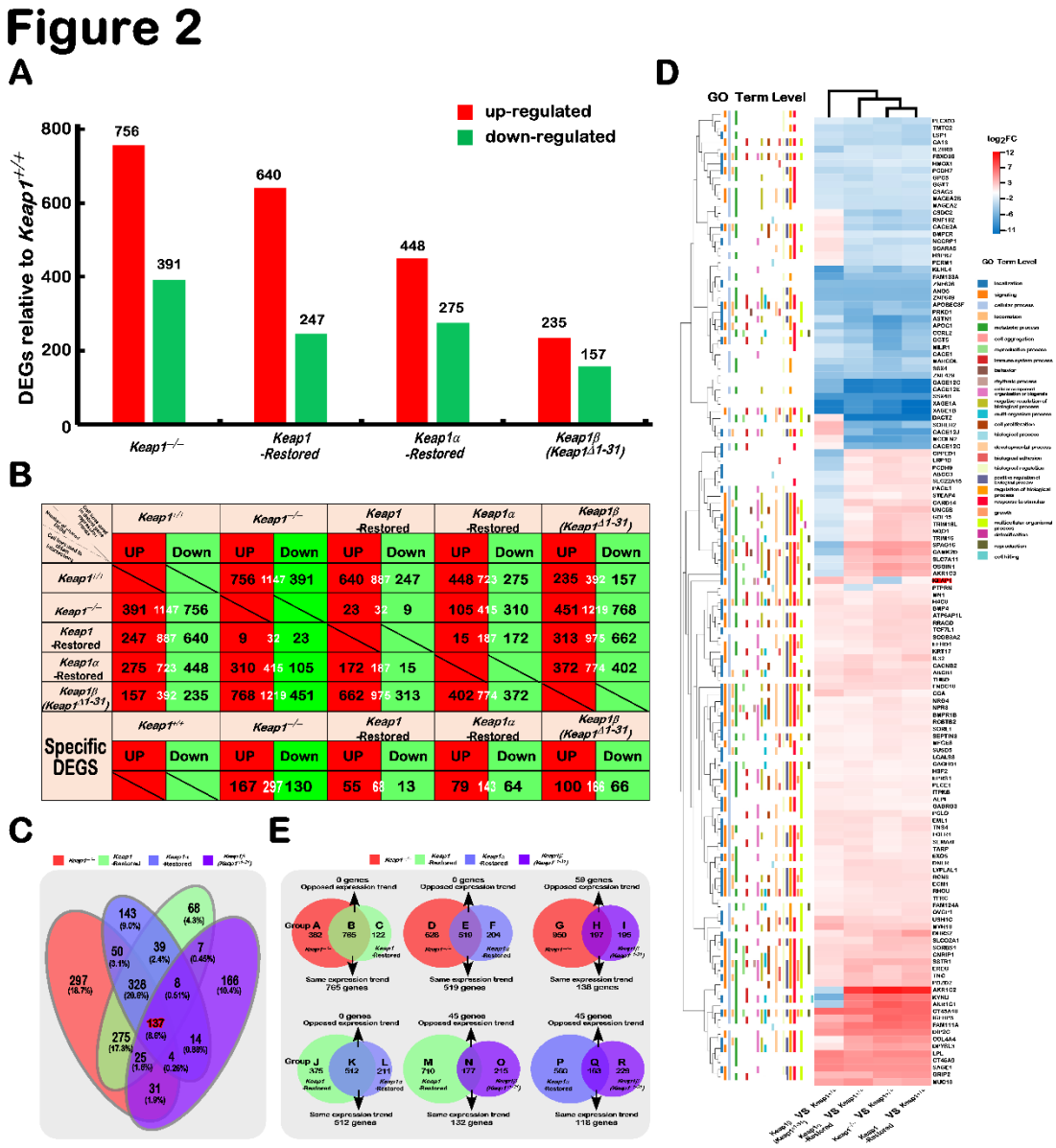

Figure 2. Statistical analysis of the data obtained from transcriptome sequencing. **(A)** The differentially expressed genes (DEGs) of different cells were analyzed by transcriptome sequencing, and the increase or decrease of the DEGs was expressed in the form of a histogram. The DEGs were selected according to the following criteria: fold change⩾2or⩽0.5 and FDR⩽0.001 (as compared to the Control cells). **(B)** The specific DEGs in each cell line and their common DEGs between every two cell lines were also counted as indicated in the chart, and the number of increased and decreased DEGs in each group is shown separately in black font, and the total is shown in white. In addition, the change trends of DEGs in each group were indicated in red or green, which represent up-regulated or down-regulated in the cells in the first row, respectively. **(C)** The common or unique DEGs among sequenced

samples were exhibited in the Venn chart. **(D)** The heatmap with hierarchical clustering of 137 DEGs shared in all four cells lines. **(E)** Venn diagrams representing common and differentially expressed genes between each two cells.

3.3. Functional annotation of specific or common DEGs in *Keap1*$^{-/-}$, *Keap1-Restored*, *Keap1α-Restored* and *Keap1β(Keap1*$^{\Delta 1-31}$*)* cells.

To gain an in-depth understanding of the similarities and differences in biological functions between *Keap1*$^{-/-}$, *Keap1-Restored*, *Keap1α-Restored* and *Keap1β(Keap1*$^{\Delta 1-31}$*)*, their common and different regulatory DEGs were identified in different combinations of each pair of groups, as indicated by Groups A to R (Figure 2E and Table S6). The same or opposite trends in those common DEGs of every two cell groups are shown. For example, 765 DEGs between *Keap1*$^{-/-}$ and *Keap1-Restored* cells had the same expression trend in Group B. In Group E, there was only one expression trend among the 595 DEGs shared between *Keap1*$^{-/-}$ and *Keap1α-Restored* cells. Two different expression trends coexisted in Group H, in which 59 DEGs expressed different trends and 138 DEGs had the same expression trend in *Keap1*$^{-/-}$ and *Keap1β(Keap1*$^{\Delta 1-31}$*)* cells. In Group K, 512 DEGs between *Keap1-Restored* and *Keap1α-Restored* cells had the same expression trend. In contrast, largely identical expression trends were observed in 132 of the common 177 DEGs coregulated by *Keap1 -Restored* and *Keap1β(Keap1*$^{\Delta 1-31}$*)* cells and in 118 of the other common 163 DEGs shared by *Keap1α-Restored* and *Keap1β(Keap1*$^{\Delta 1-31}$*)* cells in Groups N and Q.

To determine the difference between *Keap1*$^{-/-}$, *Keap1-Restored*, *Keap1α-Restored* and *Keap1β (Keap1*$^{\Delta 1-31}$*)* cells, the top 10 KEGG pathways and GO enrichment by DEGs were exhibited in scatterplots and histograms. The mRNA expression levels of selected genes were determined by q-PCR, and the putative functions of these target genes were mapped (Figure S3-S8 and Table S6). All DEGs regulated by Keap1 alone or both were divided into three groups, A, B and C, and then functionally annotated with the above-described methods (Figure S3A and Table S6). In Group A, 382 DEGs regulated by *Keap1*$^{-/-}$ cells were generally involved in signal transduction, cancer, infectious disease, transport and catabolism, metabolic processes and cellular processes. In the intersected Group B, 765 DEGs coregulated by Keap1 (*Keap1*$^{-/-}$ and *Keap1-Restored* cells) were also associated with cardiovascular disease, signal transduction, biological adhesion, metabolic process and cellular process. In Group C, 122 DEGs regulated by *Keap1-Restored* cells were significantly enriched in the cellular community, endocrine system, cancer, signal transduction, immune system process, localization and developmental process. The results of q-PCR validation (Figure S3B) revealed the expression of *AKR1C3*, *ALP1*, *GDP15*, *HPD*, *HSPB1*, *ID3*, *PGD*, *PHGDH* and *SESN2*. In addition, putative functions of such target genes were mapped, as indicated by the histogram (Figure S3B, on the bottom).

The common and distinct target DEGs in *Keap1*$^{-/-}$ and/or *Keap1α-Restored* cells were assigned to three groups. In Group D, 628 DEGs were identified as targets of *Keap1*$^{-/-}$ cells and were enriched with distinct functions in signal transduction, cellular community, infectious disease, biological regulation, metabolic process and biological regulation (Figure S4A and Table S6). Their 519 shared DEGs in Group E were functionally responsible for cancer, cardiovascular disease, signal transduction, immune system processes, biological regulation and metabolic processes. In Group F, 204 DEGs were regulated preferentially by *Keap1α-Restored* cells, and functionally associated with substance dependence, cancer, signal transduction, biological regulation, cellular processes and developmental processes. The results of q-PCR validation (Figure S4B) revealed the expression of *EPHX-1*, *HISTIHIC*, *HLA-A*, *IARS*, *SAT1*, *SESN2*, *SMAD3* and *TFRC*. The putative functions relative to these examined genes are shown (as shown in Figure 4SB, on the bottom).

Those DEGs regulated by *Keap1*$^{-/-}$ and/or *Keap1β(Keap1*$^{\Delta 1-31}$*)* in Groups G to I were functionally

annotated by DAVID, and histograms and scatterplots were constructed (Figure S5A and Table S6). Comprehensive analysis of the 10 top significant KEGG pathways and enriched biological process terms showed that 950 DEGs of Group G, from *Keap1*$^{-/-}$ cells, were associated with distinct functions in signal transduction, infectious disease, cancer, biological regulation, cellular process and developmental process, etc. In Group H, *Keap1*$^{-/-}$ and *Keap1β(Keap1*$^{\Delta 1\text{-}31}$*)*, 197 co-regulated DEGs were identified that were involved in cancer, signalling molecules and interaction, signal transduction, cellular process, metabolic process and developmental process. In Group I, only 195 DEGs were identified by transcriptional regulation by *Keap1β (Keap1*$^{\Delta 1\text{-}31}$*)* cells. Their putative functions were associated with cancer, endocrine and metabolic disease, signal transduction, biological regulation, biological adhesion, and positive regulation of biological processes. The results of q-PCR validation (Figure S5B) revealed the expression of *CD44*, *FGFBP1*, *HISTIH2BK*, *ID1*, *IL20RB*, *MYC*, *SESN2*, *SGK1*, *TALDO1* and *TFG-β1*. The putative functions relative to these examined genes are shown (as shown in Figure S5B, on the bottom).

The common and distinct target DEGs in *Keap1-Restored* and/or *Keap1α-Restored* cells were assigned to three groups. In Group J, 375 DEGs were identified as targets of *Keap1-Restored* cells and were enriched with distinct functions in cardiovascular disease, signal transduction, cell motility, cancer, immune system process, biological adhesion, metabolic process and cellular process (Figure S6A and Table S6). The 512 shared DEGs in Group K were functionally responsible for cancer, endocrine and metabolic diseases, signalling molecules and interactions, signal transduction, immune system processes, cellular processes and immune system processes. In Group L, 211 DEGs were regulated preferentially by *Keap1α-Restored* cells and functionally associated with cancer, substance dependence, cell growth and death, signal transduction, cellular processes, biological regulation and developmental processes. The results of q-PCR validation (Figure S5B) revealed the expression of CLDN1, *HLA-C*, *OPN3*, *SESN2*, *SMAD3*, *SMAD4*, *SOAT1*, *SQSTM1*, *TGF-β1* and *TNPO1* (Figure S6B). The putative functions relative to these examined genes are shown (as shown in Figure S6B, on the bottom).

All DEGs regulated by *Keap1-Restored* and/or *Keap1β(Keap1*$^{\Delta 1\text{-}31}$*)* cells were divided into Groups M to O and then functionally annotated with the above-described methods (Figure S7A and Table S6). In Group M, 710 DEGs regulated by *Keap1-Restored* cells were generally involved in signal transduction, immune system, cancer, immune system process, biological adhesion, metabolic process and developmental process. In the intersected Group N, 177 DEGs coregulated by *Keap1-Restored* and *Keap1β(Keap1*$^{\Delta 1\text{-}31}$*)* cells were also associated with development and regeneration, cancer, signal transduction, signalling molecules and interaction, signal transduction, biological adhesion, developmental process, cellular process and biological regulation. In Group O, 215 DEGs regulated by *Keap1β(Keap1*$^{\Delta 1\text{-}31}$*)* cells were significantly enriched in endocrine and metabolic disease, cancer, infectious disease, signal transduction, biological regulation, developmental process, positive regulation of biological process and cell proliferation. The results of q-PCR validation (Figure S3B) revealed that expression of *AKR1B1*,*AKR1C1*,*BLVR8*,*BMP2*,*FTL*,*G6PD*,HISTIHIC,*HLA-C*,*PI3*, *PSAT1*, *SMAD2*,*SQSTM1*,*TFRC* and *TGF-β1*(Figure S7B). In addition, putative functions of such target genes were mapped, as indicated by the histogram (Figure S7B, on the bottom).

The DEGs regulated by *Keap1α-Restored* and/or *Keap1β(Keap1*$^{\Delta 1\text{-}31}$*)* in Groups P, Q and R were functionally annotated by DAVID, and histograms and scatterplots were constructed (Figure S8A and Table S6). Comprehensive analysis of the 10 top significantly KEGG pathways and enriched biological process terms showed that 560 DEGs of Group P, in *Keap1α-Restored* cells, were associated with distinct functions in infectious disease, substance dependence, immune disease, signal transduction, immune system process, biological regulation, cellular process and developmental process. In Group Q, *Keap1α-*

Restored and *Keap1β(Keap1$^{\Delta 1-31}$)* coregulated 163 DEGs that were involved in cancer, development and regeneration, signalling molecules and interaction, endocrine and metabolic disease, developmental process, biological adhesion and cellular process. In Group R, only 229 DEGs were identified by transcriptional regulation in *Keap1β(Keap1$^{\Delta 1-31}$)* cells. Their putative functions were associated with endocrine and metabolic diseases, signal transduction, signalling molecules and interactions, cancer, biological regulation, developmental processes, cell proliferation and positive regulation of biological processes. The results of q-PCR validation (Figure S8B) revealed the expression of *CTSB*, *GARS*, *GDF15*, *HIST1H4H*, *LAMB3*, *S100A16*, *SMAD2*, *TFRC*, *TGF-β1* and *TWIST2* (Figure S8B). The putative functions relative to these examined genes are shown (as shown in Figure S8B, on the bottom).

Collectively, the genes regulated by *Keap1$^{-/-}$*, *Keap1-Restored*, *Keap1α-Restored* and *Keap1β(Keap1$^{\Delta 1-31}$)* were different, and the number of genes regulated by Keap1α was greater than that regulated by Keap1β. A comprehensive analysis of the four cell lines found the same following functions in KEGG pathways and GO enrichment: cancer, signal transduction, signalling molecules and interaction, biological regulation, cellular process and developmental process. There were also different KEGG pathways and GO enrichment functions: cellular community, endocrine system, immune system, infectious disease, localization, immune system process and response to stimulus. Notably, both PI3K-mTOR pathways were found in the KEGG pathway analysis.

3.4. Knockout of *Keap1* was a more potent player than *Keap1β(Keap1$^{\Delta 1-31}$)* at preventing tumour xenografts in nude mice.

To investigate the effect of deletion of all Keap1 or Keap1α alone on tumour growth, *Keap1$^{+/+}$* (wild-type, WT), *Keap1$^{-/-}$* and *Keap1β (Keap1$^{\Delta 1-31}$)* cells were heterotransplanted into groups of immunodeficient nude mice at their subcutaneous loci as indicated. After tumour formation, the sizes of growing tumours were measured at one-day intervals within the ensuing 25 days before the tumour-bearing mice were sacrificed. The resulting data (tumour, size and weight) were calculated and graphed. The resulting images showed that the carcinomas derived from *Keap1$^{+/+}$* cells were estimated to be ~7.0 times in tumour volume and weight larger than those of *Keap1$^{-/-}$* cells and 3.0 times that of *Keap1β(Keap1$^{\Delta 1-31}$)* cells (Figure 3A-C). The fact that carcinomas derived from *Keap1β* were larger than carcinomas derived from Keap1$^{+/+}$ and litter than carcinomas derived from Keap1$^{-/-}$ demonstrates that *Keap1* and *Keap1β(Keap1$^{\Delta 1-31}$)* can promote the occurrence and development of tumours.

Then, xenograft tumours were subjected to histopathological examination (HE) by routine haematoxylin-eosin staining, followed by immunohistochemical staining with antibodies against Keap1 and PTEN (Figure S9). Through HE staining experiments, we found that some cell necrosis and liquefaction occurred in the tumours formed by *Keap1$^{+/+}$* and *Keap1β(Keap1$^{\Delta 1-31}$)* cells, among which *Keap1$^{+/+}$* cells had more necrosis, while there were almost no tumours formed by Keap1$^{-/-}$ cells (Figure S9A). In the tumour-bearing tissue formed by *Keap1$^{-/-}$* cells, the overall colouration of the cells was darker, and there were a large number of cancer grooves in the formed tumours to wrap the tumour cells.

When compared with *Keap1$^{+/+}$* cells, Keap1 expression was markedly decreased in *Keap1$^{-/-}$* cell-derived tumour tissue and markedly increased in *Keap1β(Keap1$^{\Delta 1-31}$)* cell-derived tumour tissue (Figure S9B). Further immunohistochemistry of the tumour-specific marker PTEN revealed significant enhancements of PTEN in *Keap1$^{-/--}$* and *Keap1β(Keap1$^{\Delta 1-31}$)* derived xenograft tissues (Figure S9C).

Furthermore, a series of comparative experiments revealed that *Keap1$^{-/-}$* and *Keap1β (Keap1$^{\Delta 1-31}$)* cell proliferation levels were significantly suppressed compared with *Keap1$^{+/+}$* cell proliferation (Figure 3D).

Figure 3

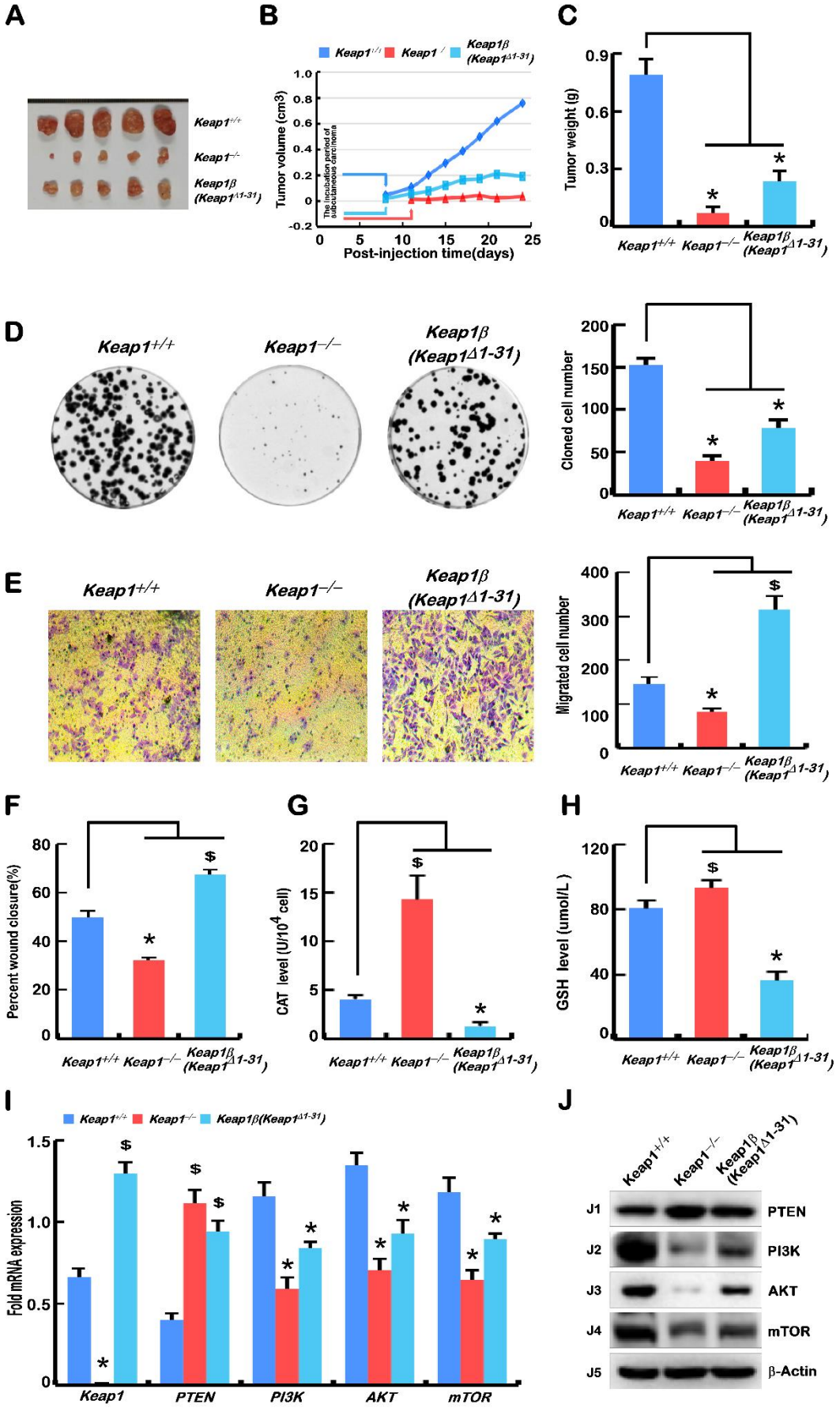
A
Keap1+/+
Keap1−/−
Keap1β (Keap1Δ1-31)
B
Keap1+/+ Keap1−/− Keap1β (Keap1Δ1-31)
Tumor volume (cm3)
The incubation period of subcutaneous carcinoma
Post-injection time(days)
C
Tumor weight (g)
Keap1+/+ Keap1−/− Keap1β (Keap1Δ1-31)
D
Keap1+/+
Keap1−/−
Keap1β (Keap1Δ1-31)
Cloned cell number
E
Keap1+/+
Keap1−/−
Keap1β (Keap1Δ1-31)
Migrated cell number
F
Percent wound closure(%)
G
CAT level (U/10^4 cell)
H
GSH level (umol/L)
I
Keap1+/+ Keap1−/− Keap1β(Keap1Δ1-31)
Fold mRNA expression
Keap1
PTEN
PI3K
AKT
mTOR
J
Keap1+/+
Keap1−/−
Keap1β (Keap1Δ1-31)
J1 PTEN
J2 PI3K
J3 AKT
J4 mTOR
J5 β-Actin

Figure 3. Knockout of Keap1 was a more potent player than Keap1β(Keap1$^{\triangle 1\text{-}31}$) at preventing tumour xenografts in nude mice. **(A)** Subcutaneous tumor formation in nude mice. *Keap1$^{+/+}$*, *Keap1$^{-/-}$* and *Keap1β(Keap1$^{\Delta 1\text{-}31}$)* cells were injected subcutaneously in nude mice, and 5 mice were injected with each cell, and the tumors were fetched out after 25 days. **(B)** Tumor growth curves of *Keap1$^{+/+}$*, *Keap1$^{-/-}$* and *Keap1β(Keap1$^{\Delta 1\text{-}31}$)* cells in subcutaneous tissues of nude mice within 25 days. **(C)** Remove the tumor from the subcutaneous area of nude mice and weigh its mass. **(D)** Cell proliferation was detected by the colony-forming unit assays. the same amount of *Keap1$^{+/+}$*, *Keap1$^{-/-}$* and *Keap1β(Keap1$^{\Delta 1\text{-}31}$)* cells were cultured in capsule, and the corresponding number of clones was recorded after 10 days. The number of clones of each dish was quantified. **(E)** Transwell migration assays. The polycarbonate film stained with crystal violet was photographed on inverted microscope. The number of cells migrated across the membrane in *Keap1$^{+/+}$*, *Keap1$^{-/-}$* and *Keap1β(Keap1$^{\Delta 1\text{-}31}$)* cells were calculated. **(F)** Wound healing assay. According to the scratch width in Figure S10A and S10B, the cell mobility of each cells was calculated at 24h, 48h and72h. **(G)** Calculate the CAT of *Keap1$^{+/+}$*, *Keap1$^{-/-}$* and *Keap1β(Keap1$^{\Delta 1\text{-}31}$)* cells according to the kit instructions. **(H)** Calculate the GSH of *Keap1$^{+/+}$*, *Keap1$^{-/-}$* and *Keap1β(Keap1$^{\Delta 1\text{-}31}$)* cells according to the kit instructions. (**I)** Q-PCR was used to detect the mRNA expressions of *Keap1*, *PTEN*, *PI3K*, *AKT* and *mTOR* in *Keap1$^{+/+}$*, *Keap1$^{-/-}$* and *Keap1β(Keap1$^{\Delta 1\text{-}31}$)* cells. **(J)** WB was used to detect the protein expressions of Keap1, PTEN, PI3K, AKT and mTOR in *Keap1$^{+/+}$*, *Keap1$^{-/-}$* and *Keap1β(Keap1$^{\Delta 1\text{-}31}$)* cells. N≥3, and "*" "$" indicates p≤0.01.

Cell cycle results showed *Keap1$^{-/-}$* cells underwent cycle arrest at G1, which contributes to tumour reduction, and the cycle of *Keap1β* cells did not change significantly (Figure S10C). Meanwhile, apoptosis of *Keap1$^{-/-}$* and *Keap1β* cells increased (Figure S10D). Further experiments showed that the invasion and migration of *Keap1$^{-/-}$ cells* were inhibited, while those of *Keap1β(Keap1$^{\Delta 1\text{-}31}$)* cells were promoted (Figure 3E, 3F, S10A, S10B). The relevant data were measured by CAT and GSH kits, and the results showed that, compared with *Keap1$^{+/+}$* cells, *Keap1$^{-/-}$* cells were increased, while *Keap1β(Keap1$^{\Delta 1\text{-}31}$)* cells were decreased (Figure 3G, 3H). Based on the xenograft tumour results, qPCR and WB experiments were performed on the tumour marker PTEN-mTOR pathway. The results in *Keap1$^{-/-}$* and *Keap1β(Keap1$^{\Delta 1\text{-}31}$)* cells showed that *PTEN* was enhanced, and *PI3K*, *AKT* and *mTOR* were all decreased (Figure 3I, 3J), showing the same trends as tumours (Figure 3A-C). However, their changes (increased or decreased) were more pronounced in the Keap1 cell line. *Keap1 and Keap1β* acted as more potent tumour promoters, albeit both isoforms were endowed with an intrinsic capability to prevent tumour development and malgrowth.

3.5. Malgrowth of *Keap1$^{-/-}$*derived hepatoma cells was significantly suppressed by the restoration of *Keap1α*, and the *Keap1-Restored* promoted their growth.

To further explore the effects of Keap1 and Keap1α on tumour growth, both *Keap1-Restored* and *Keap1α-Restored* cells, alongside *Keap1$^{-/-}$* (WT) cells, were heterotransplanted into groups of immunodeficient nude mice at their subcutaneous loci as indicated. After tumour formation, the sizes of growing tumours were measured at one-day intervals within the ensuing 30 days before the tumour-bearing mice were sacrificed. The resulting data (tumour size and weight) were calculated and are shown graphically. The results obtained were as follows: the human carcinoma derived from *Keap1$^{-/-}$* cell tumours were estimated to be 0.3 times larger than those derived from *Keap1-Restored* cells and 4.0 times larger than those derived from *Keap1α-Restored* cells (Figure 4A-C). These results further demonstrate the role of Keap1 in promoting tumour growth; however, it is surprising that Keap1α has the opposite effect on tumour growth as Keap1 and can promote tumour growth.

Then, xenograft tumours were subjected to histopathological examination by routine haematoxylin-eosin staining, followed by immunohistochemical staining with antibodies against Keap1 and PTEN (Figure S11). The results of HE staining showed that some cell necrosis and liquefaction occurred in the tumour body formed by *Keap1$^{-/-}$*, *Keap1-Restored* and *Keap1α-Restored* cells (Figure S11A). Compared with tumours formed by *Keap1$^{-/-}$* cells, in the tumour-bearing tissue formed by *Keap1-Restored* and *Keap1α-Restored* cells, the overall colouration of the cells was darker, the cells were more basophilic, and there were a large number of cancer grooves in the tumour formed by *Keap1α-Restored*

Figure 4

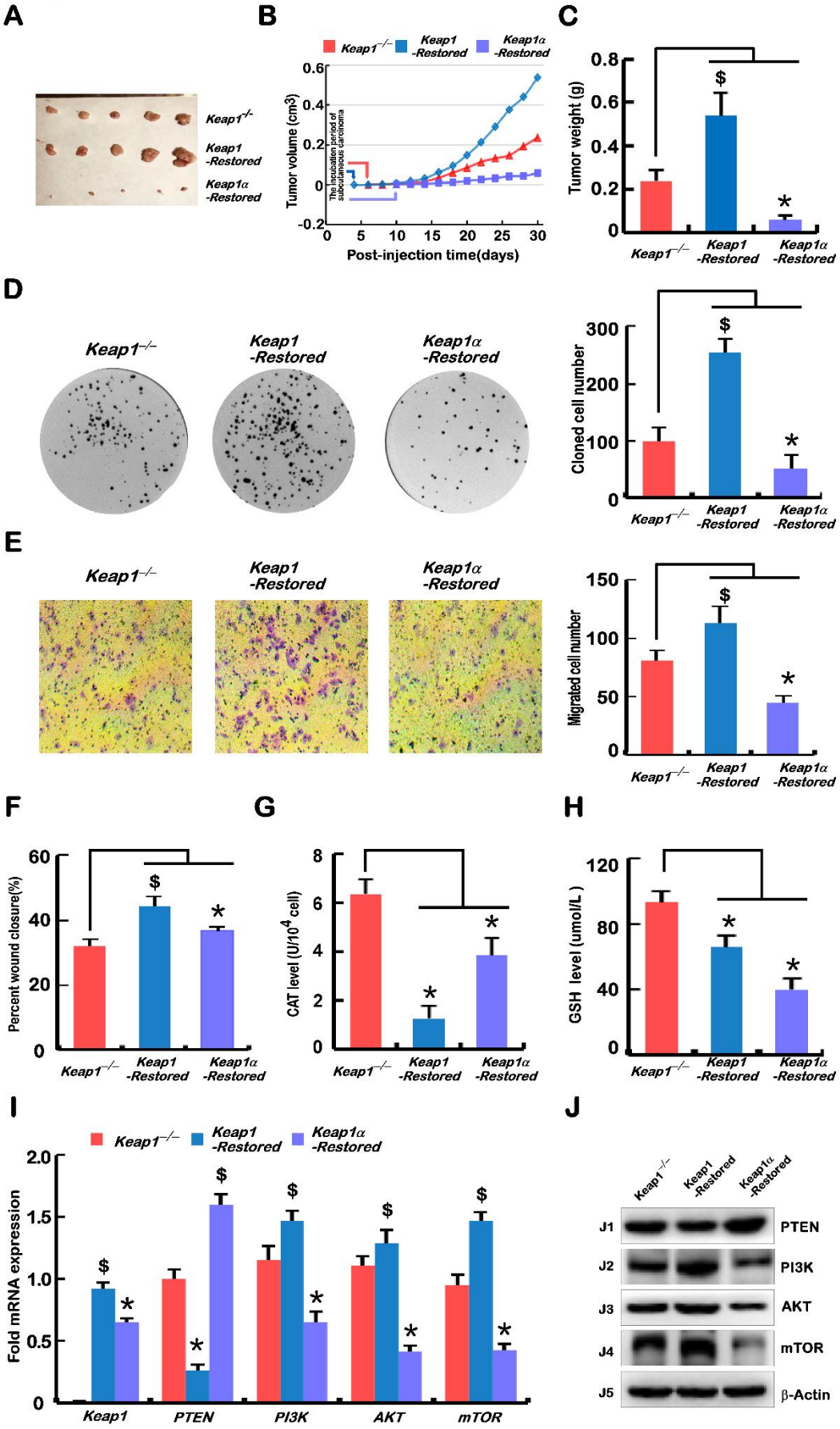
A
Keap1-/-
Keap1 -Restored
Keap1α -Restored
B
Keap1-/-
Keap1 -Restored
Keap1α -Restored
Tumor volume (cm3)
The incubation period of subcutaneous carcinoma
Post-injection time(days)
C
Tumor weight (g)
D
Cloned cell number
E
Migrated cell number
F
Percent wound closure(%)
G
CAT level (U/10^4 cell)
H
GSH level (umol/L)
I
Fold mRNA expression
Keap1
PTEN
PI3K
AKT
mTOR
J
J1 PTEN
J2 PI3K
J3 AKT
J4 mTOR
J5 β-Actin

Figure 4. Malgrowth of Keap1$^{-/-}$ derived hepatoma cells were significantly suppressed by restoration of Keap1α, and the Keap1-Restored can promote their growth. **(A)** Subcutaneous tumor formation in nude mice. *Keap1$^{-/-}$*, *Keap1-Restored* and *Keap1α-Restored* cells were injected subcutaneously in nude mice, and 5 mice were injected with each cell, and the tumors were fetched out after 30 days. **(B)** Tumor growth curves of *Keap1$^{-/-}$*, *Keap1-Restored* and *Keap1α-Restored* cells in subcutaneous tissues of nude mice within 30 days. **(C)** Remove the tumor from the subcutaneous area of nude mice and weigh its mass. **(D)** Cell proliferation was detected by the colony-forming unit assays. The same amount of *Keap1$^{-/-}$*, *Keap1-Restored* and *Keap1α-Restored* cells were cultured in capsule, and the corresponding number of clones was recorded after 10 days. The number of clones of each dish was quantified. **(E)** Transwell migration assays. The polycarbonate film stained with crystal violet was photographed on inverted microscope. The number of cells migrated across the membrane in *Keap1$^{-/-}$*, *Keap1-Restored* and *Keap1α-Restored* cells were calculated. **(F)** Wound healing assay. According to the scratch width in figure S12A and S12B, the cell mobility of each cells was calculated at 24h, 48h and72h. **(G)** Calculate the CAT of *Keap1$^{-/-}$*, *Keap1-Restored* and *Keap1α-Restored* cells according to the kit instructions. **(H)** Calculate the GSH of *Keap1$^{-/-}$*, *Keap1-Restored* and *Keap1α-Restored* cells according to the kit instructions. (**I)** Q-PCR was used to detect the mRNA expressions of *Keap1*, *PTEN*, *PI3K*, *AKT* and *mTOR* in *Keap1$^{-/-}$*, *Keap1-Restored* and *Keap1α-Restored* cells. **(J)** WB was used to detect the protein expressions of Keap1, PTEN, PI3K, AKT and mTOR in *Keap1$^{-/-}$*, *Keap1-Restored* and *Keap1α-Restored* cells. N≥3, and "*" "$" indicates p≤0.01.

cells, which inhibited the growth of the tumour (Figure S11A). When compared with tumours formed by *Keap1$^{-/-}$* cells, immunohistochemistry of the tumour-specific markers (Keap1) revealed significant enhancements of Keap1 in the *Keap1-Restored* and *Keap1α-Restored* derived xenograft tissues (Figure S11B), and the expression of PTEN was markedly decreased in the *Keap1-Restored* cell-derived tumour tissue and was markedly increased in the *Keap1α-Restored* cell-derived tumour tissue (Figure S11C).

Further results showed that *Keap1$^{-/-}$* cell proliferation, invasion and migration were all significantly promoted by the restoration of *Keap1*, while *Keap1α-Restored* cells were significantly suppressed (Figure 4D-F, S12A, S12B). In *Keap1-Restored* cell, the G1 phase of the cell cycle was shortened (Figure S12C). Meanwhile, the restoration of *Keap1* reduced apoptosis, and the restoration of *Keap1α* significantly increased apoptosis (Figure S12D). The relevant data were measured by CAT and GSH kits, and the results showed that, compared with *Keap1$^{-/-}$* cells, *Keap1-Restored* and *Keap1α-Restored* cells were decreased (Figure 4G, 4H). The expression of the tumour-specific marker pathway (PTEN-mTOR pathway) was verified by q-PCR and WB. The results in the *Keap1-Restored* cells showed that *PTEN* was inhibited, and *PI3K*, *AKT* and *mTOR* were promoted, but the *Keap1α-Restored* cells had a completely opposite trend (Figure 4I, 4J). Their phenotypes were verified by qPCR and WB in xenograft tumours (Figure 4A-C). As a consequence, the restoration of Keap1α enabled a significant tumour-preventing effect on subcutaneous human carcinoma xenografts in nude mice, but the recovery of Keap1 promoted the tumour effect.

Collectively, *Keap1* acts as a potent tumour promoter, and isoform α can prevent tumour development and malgrowth.

3.6. Deficiency of Keap1 and its subtypes (α and β) results in dysregulation of genes controlling cell behaviour.

The aforementioned results demonstrated that loss of Keap1 and its subtypes (α and β) led to marked phenotypic changes in cell behaviour, such as tumorigenesis of the derived carcinoma xenografts, and growth, invasion, migration, transformation, cycle and apoptosis from *Keap1$^{+/+}$*, *Keap1$^{-/-}$*, *Keap1-Restored*, *Keap1α-Restored cells* and *Keap1β(Keap1$^{\Delta 1-31}$)*. The subset of genes that control cell processes and behaviours was dysregulated in several cells, and we performed q-PCR and WB to identify them.

In the epithelial-mesenchymal transition (EMT) test experiments, *Keap1$^{+/+}$* cells were used as a control. As anticipated in Figure 5A and 5B, the results revealed the upregulation of key genes encoding the epithelial marker proteins *CTNNA1 (α-Catenin)*, *CTNNB1 (β-Catenin)* and *CDH1* in *Keap1$^{-/-}$* cells. The

upregulation of *CTNNA1*, *CTNNB1* and *CDH1* was accompanied by the downregulation of critical genes encoding the mesenchymal marker proteins *CDH2*, *FN1* and vimentin. Then, the expression levels of zinc finger transcription factors (*SNAI1* and *SNAI2*) were reduced. *SNAI1* and *SNAI2* have been shown to act as key mediators of EMT by regulating the expression of the target genes *CDH1* and *CDH2* by binding the E-boxes in their promoter regions, particularly in metastatic hepatocellular carcinoma[19,25,26]. Moreover, loss of Keap1 also downregulated the transcriptional (and translational) expression of genes encoding membrane-type *MMP17* and matrix metallopeptidase 9 (MMP9) in *Keap1*$^{-/-}$ cells. However, *Keap1β(Keap1*$^{\Delta 1\text{-}31}$*)* cells showed completely opposite results to *Keap1*$^{-/-}$ cells. Compared with *Keap1*$^{-/-}$ cells, q-PCR was used to detect typical genes related to EMT in the *Keap1-Restored* and *Keap1α-Restored* cells. In the *Keap1-Restored* cells, the *CTNNA1*, *CTNNB1* and *CDH1* genes were found to be downregulated, while the remaining genes were enhanced (Figure 5C). However, the *Keap1α-Restored* cells demonstrated the opposite results of the *Keap1-Restored* cells. In these cells (Keap1$^{-/-}$, *Keap1-Restored* and *Keap1α-Restored cells*), WB and q-PCR experiments showed the same trends (Figure 5D).

3.7. Knockout of Keap1 and its subtypes (α and β) results in dysregulation of genes controlling the cell cycle and apoptosis.

To gain insight into the abovementioned cell cycle and apoptosis changes from the mechanism, q-PCR was performed to detect the deletion of Keap1 and its subtypes to identify the key cycle and apoptosis genes involved. As anticipated, the expression levels of *P53*, *P21* and *CDK2* were significantly downregulated in *Keap1*$^{-/-}$ and *Keap1β (Keap1*$^{\Delta 1\text{-}31}$*)* cells compared with equivalent values obtained from *Keap1*$^{+/+}$ control cells (Figure 4E). These findings supported the view that the S phases of *Keap1*$^{-/-}$ and *Keap1β(Keap1*$^{\Delta 1\text{-}31}$*)* cells were reduced. Intriguingly, *Keap1*$^{-/-}$ and *Keap1β(Keap1*$^{\Delta 1\text{-}31}$*)* cells upregulated the mRNA expression levels of genes encoding *CDK6* and *Cyclin D1* (both were involved in a functional complex controlling the G1-S transition) in *Keap1*$^{-/-}$ and *Keap1β(Keap1*$^{\Delta 1\text{-}31}$*)* cells (Figure 5E). In addition, proapoptotic genes (e.g., *Caspases 3*, *4* and *6*) were increased, while antiapoptotic genes (e.g., *Bcl2* and *Bcl2l1*) were decreased in *Keap1*$^{-/-}$ and *Keap1β(Keap1*$^{\Delta 1\text{-}31}$*)* cells when *Keap1*$^{+/+}$ cells were used as a reference (Figure 5F). To verify the effects of Keap1 on cell cycle progression and apoptosis, *Keap1-Restored* and *Keap1α-Restored* cells were compared to *Keap1*$^{-/-}$ cells to determine the real-time PCR expression levels of related genes. Upregulation of the *P53-P21-CDK2* signalling pathway by *Keap1-Restored* and *Keap1α-Restored* cells led to an increase in the S phase of cells; however, *CDK6* and *CyclinD*1 were both decreased (Figure 5G). Apoptosis-related genes were also tested. Genes (e.g., *Caspases 3*, *4* and *6*) that promote apoptosis were decreased, and genes (e.g., *Bcl2* and *Bcl2l1*) that resist apoptosis were increased in the *Keap1-Restored* cells, but proapoptotic and antiapoptotic genes showed the opposite trends in *Keap1α-Restored* cells (Figure 5H).

Figure 5

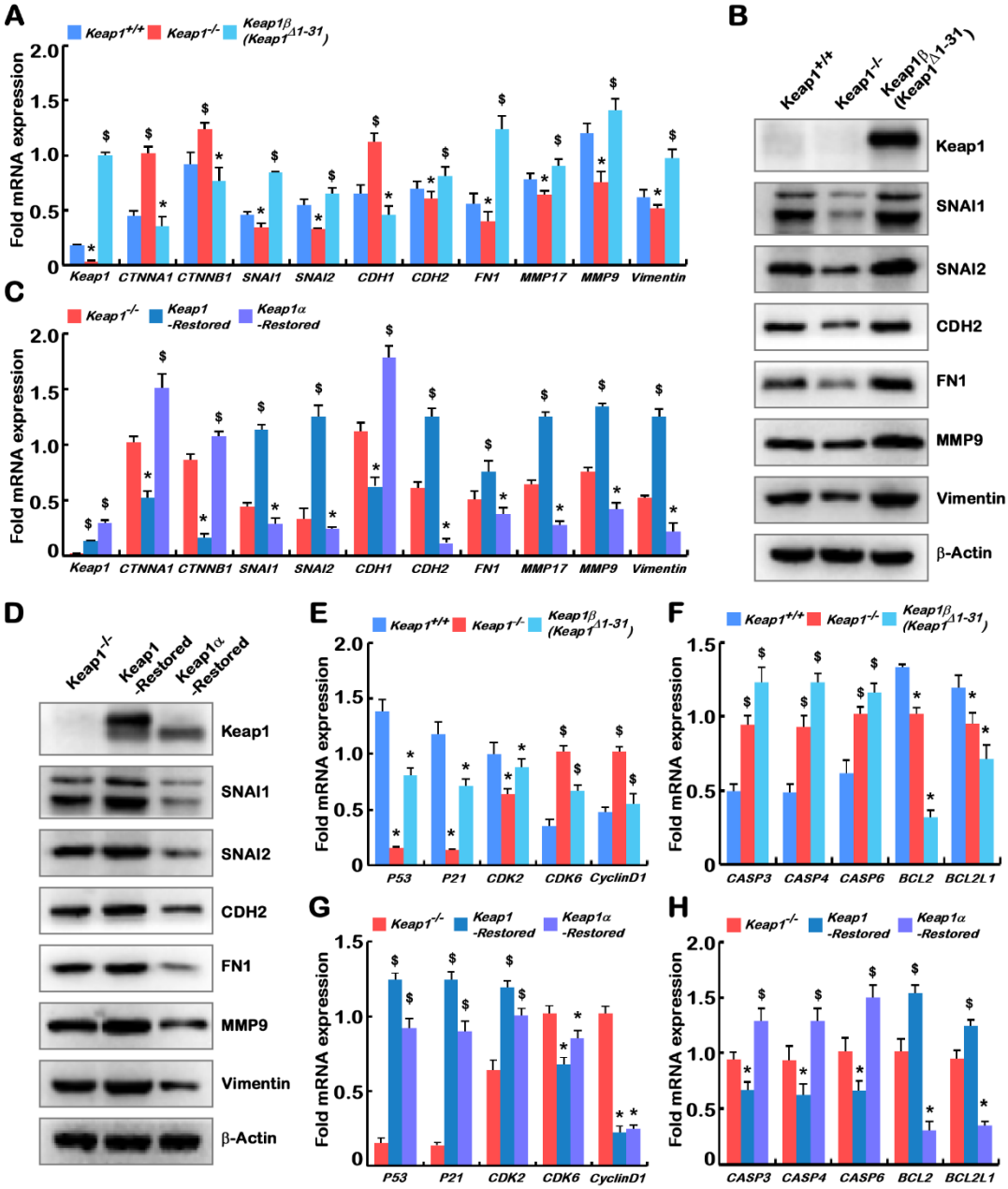

Figure 5. Deficiency of Keap1 and its isoforms (α and β) lead to genetic dysregulation of cell behavior, cycle and apoptosis. (**A**) Q-PCR was used to detect the mRNA expressions of *Keap1, CTNNA1, CTNNB1, SNAI1, SNAI2, CDH1, CDH2, FN1, MMP17, MMP9* and *Vimentin* in *Keap1*$^{+/+}$, *Keap1*$^{-/-}$ and *Keap1β(Keap1*$^{\Delta 1\text{-}31}$*)* cells. (**B**) WB was used to detect the protein expressions of *Keap1*, *CTNNA1*, *CTNNB1*, *SNAI1*, *SNAI2*, *CDH1*, *CDH2*, *FN1*, *MMP17*, *MMP9* and *Vimentin* in *Keap1*$^{+/+}$, *Keap1*$^{-/-}$ and *Keap1β(Keap1*$^{\Delta 1\text{-}31}$*)* cells. (**C**) Q-PCR was used to detect the mRNA expressions of *Keap1, CTNNA1, CTNNB1, SNAI1, SNAI2, CDH1, CDH2, FN1, MMP17, MMP9* and *Vimentin* in *Keap1*$^{-/-}$, *Keap1-Restored* and *Keap1α-Restored* cells. (**D**) WB was used to detect the protein expressions of *Keap1*, *CTNNA1*, *CTNNB1*, *SNAI1*, *SNAI2*, *CDH1*, *CDH2*, *FN1*, *MMP17*, *MMP9* and *Vimentin* in *Keap1*$^{-/-}$, *Keap1-Restored* and *Keap1α-Restored* cells. (**E**) Q-PCR was used to detect the mRNA expressions of *P53, P21, CDK2, CDK6* and *CyclinD1* in *Keap1*$^{+/+}$, *Keap1*$^{-/-}$ and *Keap1β(Keap1*$^{\Delta 1\text{-}31}$*)* cells. (**F**) Quantitative real-time PCR was used to detect the mRNA expressions of *CASP3*, *CASP4*, *CASP6*, *BCL2* and *BCL2L1* in *Keap1*$^{+/+}$, *Keap1*$^{-/-}$ *and Keap1β(Keap1*$^{\Delta 1\text{-}31}$*)* cells. (**G**) Q-PCR was used to detect the mRNA expressions of *P53*, *P21*, *CDK2*, *CDK6* and *CyclinD1* in *Keap1*$^{-/-}$, *Keap1-Restored* and *Keap1α-Restored* cells. (**H**) Q-PCR was used to detect the mRNA expressions of *CASP3*, *CASP4*, *CASP6*, *BCL2* and *BCL2L1* in *Keap1*$^{-/-}$, *Keap1-Restored* and *Keap1α-Restored* cells. N≥3, and "*" "$" indicates p≤0.01.

4. Discussion

In the present study, we established four controllable cell models for stably expressing *Keap1*$^{-/-}$, *Keap1β(Keap1*$^{\Delta 1-31}$*)*, *Keap1-Restored* or *Keap1α-Restored*, which all occur naturally with their respective intact structural domains. Of striking note, the two isoforms of Keap1 (α and β) were mainly affected by the expression of the N-terminal amino acids 1 and 32, respectively (Figure 1A-D). It has been reported that the DC domain of Keap1 can directly interact with the carboxy-terminal Neh2 of Nrf2[1]. Overexpression of Keap1a and Keap1b in embryos showed no significant difference in the inhibition of Nrf2[27]. Our results also showed that two isoforms of Keap1 (α and β) bind to Nrf2 in the cytoplasm and inhibit the expression of Nrf2 and its target gene (HO-1) in cancer cells (Figure 1E-J). In zebrafish, studies showed that Keap1a knockout and Keap1b knockout had certain differences in genes and pathways and were identified by RNA-seq analysis[4]. According to the analysis of transcriptome sequencing results, it was found that the deletion and restoration of Keap1, Keap1α and Keap1β had different regulated genes, among which Keap1 regulated the most and Keap1β the least (Figure 2A, 2B). Venn diagrams and cluster heatmaps were compared, and it was again verified that Keap1 and its isoforms (α and β) had different regulatory functions (Figure 2C-E). The top 10 KEGG pathways and GO enrichment were analysed, and after pairwise comparison, it was found that these cells had similar or different biological processes. Notably, the PI3K-mTOR pathway had been repeatedly identified in cell line transcriptome data analysis (KEGG pathways), suggesting that Keap1 and its isoforms (α and β) had a regulatory role in this pathway (Figure S2-S8).

The role of Keap1 deletion and subsequent Nrf2 activation is highly debated in the scientific community. Keap1 loss-of-function mutations or Nrf2 gain-of-function mutations were predictors of poor clinical outcome in different tumour aetiologies, such as in HCC and ovarian, lung, endometrial, breast, and head and neck cancers[28,29]. For HCC, it has been reported that mutations in Keap1 or Nrf2 have been detected in approximately 12% of cases[29,30], implying that an active Keap1-Nrf2 pathway could induce or drive the development of HCC. The study showed that a mouse model constructed with Keap1 knockout in the liver had smaller tumours[29]. Of note, our data showed that Keap1$^{-/-}$ mice developed fewer and smaller tumours than *Keap1*$^{+/+}$ mice, with a lower tumour frequency in nude mouse subcutaneous tumour transplantation experiments (Figure 3A-C). Additionally, we found that tumours recovered by *Keap1α-Restored* cells were smaller than those recovered by *Keap1*$^{-/-}$ cells (Figure 4A-C). This suggests that complete Keap1 promotes tumour growth, but as Keap1 isoforms, Keap1a inhibits tumour growth, and Keap1b promotes tumour growth. The opposite effects of different subtypes of Keap1 and the different proportions of different subtypes in different tissues may be the reason why Keap1 plays tumour-promoting and tumour-suppressing roles in different tissues. In vitro experiments (cell clones) also confirmed that the deletion of Keap1 or Keap1 isoforms (α or β) inhibited tumour formation (Figure 3D, 4D).

More than 90% of cancer deaths are related to tumour cell metastasis[31], and EMT is considered to lead to invasion and metastasis during the malignant transformation of liver cancer[32,33]. Deletion of Keap1 inhibited the in vitro migration and invasion of cancer cells, whereas Keap1β expression alone showed the opposite result (Figure 3E, 3F, S10A, S10B). Restoring Keap1 promoted the in vitro migration and invasion of cancer cells, whereas Keap1α expression alone had the opposite effect (Figure 4E, 4F, S12A, S12B). The above experimental results showed that the EMT behaviour of cells was changed. The reason was that Keap1 and its isoforms (α or β) affected cell migration and the expression of adhesion junction genes (Figure 5A-D). In our experiments, we found that Keap1 and its isoforms (α and β) had different effects. Deletion of Keap1 activated the expression of CAT and GSH;

when only Keap1 isoforms (α or β) were present, their expression was suppressed (Figure 3G, 3H, 4G, 4H). The experimental results showed that Keap1 and its isoforms (α and β) had opposite regulatory effects on these activities.

The formation of tumours is affected by many factors, among which the PTEN and PI3K-AKT-mTOR pathways have been studied in more depth. PTEN is a typical tumour suppressor that inhibits the expression of the PI3K-mTOR pathway, regulates cell proliferation, apoptosis, protein synthesis and glucose metabolism, and promotes tumour progression[34]. Overexpression of PI3K in hepatocytes could lead to steatosis and lipid accumulation, accelerating tumour formation[35,36]. We obtained the same experimental results by immunohistochemistry (Figure S9C, S11C), q-PCR (Figure 3I, 4I) and WB (Figure 3J, 4J) experiments. More specifically, the PI3K/AKT/mTOR signalling pathway could induce tumour initiation and cell expansion by regulating cell cycle progression[37,38]. A series of comparative experiments showed that the S phase of *Keap1*$^{-/-}$ cells was the shortest, and the S phase was slightly increased when only *Keap1α-Restored* or *Keap1β(Keap1*$^{\Delta 1-31}$*)* cells were present (Figure S10C, S12C). Our results also showed that the deletion of Keap1 or the presence of an isoform (α or β) significantly increased the apoptosis rate, and the apoptosis rate was the highest when only isoform α was present (Figure S10D, S12D). Meanwhile, our results also found that Keap1 and its isoforms (α and β) deregulated the expression levels of cell cycle and apoptosis genes (Figure 5E-H). The results were basically consistent with the results of in vitro experiments (measurements of the cell cycle and apoptosis by flow cytometry). Therefore, we believe that Keap1 and its isoforms (α and β) affect the expression of cell cycle- and apoptosis-related genes by activating the PTEN and PI3K-mTOR pathways.

In summary, we provide compelling in vitro and in vivo evidence demonstrating that Keap1 and its subtypes (α and β) have similar and different functions in tumour formation, regulation of EMT, cell cycle progression and apoptosis of metastatic cells. It should be noted that the effects of Keap1 deletion and subsequent activation of Nrf2 are different in different tumour models, and the results are still controversial.

Author Contributions: F.C. performed the experiments with help of M.X., J.F., R.W., K.L. and S.H., collected all the relevant data, and wrote a draft of this manuscript with most figures and supplemental information. Y.Z. designed and supervised this study, analyzed all the data, helped to prepare all figures with cartoons, and wrote and revised the paper with help of G.S. All cauthors have read and agreed to the published version of the manuscript.

Funding: This study was funded by the National Natural Science Foundation of China (NSFC, with a key program 91429305 and other two projects 81872336 and 82073079) awarded to Prof. Yiguo Zhang (at Chongqing University).

Acknowledgments: We thank all other present and past members of Zhang's laboratory (at Chongqing University, China) for giving critical discussion and invaluable help with this work.

References

1. Itoh, K.; Wakabayashi, N.; Katoh, Y.; Ishii, T.; Igarashi, K.; Engel, J.D.; Yamamoto, M. Keap1 represses nuclear activation of antioxidant responsive elements by Nrf2 through binding to the amino-terminal Neh2 domain. *Genes Dev* **1999**, *13*, 76-86, doi:10.1101/gad.13.1.76.
2. Panieri, E.; Telkoparan-Akillilar, P.; Suzen, S.; Saso, L. The NRF2/KEAP1 Axis in the Regulation of Tumor Metabolism: Mechanisms and Therapeutic Perspectives.

Biomolecules **2020**, *10*, doi:10.3390/biom10050791.
3. Qiu, L.; Wang, M.; Zhu, Y.; Xiang, Y.; Zhang, Y. A Naturally-Occurring Dominant-Negative Inhibitor of Keap1 Competitively against Its Negative Regulation of Nrf2. *Int J Mol Sci* **2018**, *19*, doi:10.3390/ijms19082150.
4. Nguyen, V.T.; Bian, L.; Tamaoki, J.; Otsubo, S.; Muratani, M.; Kawahara, A.; Kobayashi, M. Generation and characterization of keap1a- and keap1b-knockout zebrafish. *Redox Biol* **2020**, *36*, 101667, doi:10.1016/j.redox.2020.101667.
5. Hayes, J.D.; McMahon, M. NRF2 and KEAP1 mutations: permanent activation of an adaptive response in cancer. *Trends Biochem Sci* **2009**, *34*, 176-188, doi:10.1016/j.tibs.2008.12.008.
6. Hast, B.E.; Cloer, E.W.; Goldfarb, D.; Li, H.; Siesser, P.F.; Yan, F.; Walter, V.; Zheng, N.; Hayes, D.N.; Major, M.B. Cancer-derived mutations in KEAP1 impair NRF2 degradation but not ubiquitination. *Cancer Res* **2014**, *74*, 808-817, doi:10.1158/0008-5472.CAN-13-1655.
7. Moi, P.; Chan, K.; Asunis, I.; Cao, A.; Kan, Y.W. Isolation of NF-E2-related factor 2 (Nrf2), a NF-E2-like basic leucine zipper transcriptional activator that binds to the tandem NF-E2/AP1 repeat of the beta-globin locus control region. *Proc Natl Acad Sci U S A* **1994**, *91*, 9926-9930, doi:10.1073/pnas.91.21.9926.
8. Itoh, K.; Igarashi, K.; Hayashi, N.; Nishizawa, M.; Yamamoto, M. Cloning and characterization of a novel erythroid cell-derived CNC family transcription factor heterodimerizing with the small Maf family proteins. *Mol Cell Biol* **1995**, *15*, 4184-4193, doi:10.1128/MCB.15.8.4184.
9. Vomund, S.; Schafer, A.; Parnham, M.J.; Brune, B.; von Knethen, A. Nrf2, the Master Regulator of Anti-Oxidative Responses. *Int J Mol Sci* **2017**, *18*, doi:10.3390/ijms18122772.
10. Itoh, K.; Chiba, T.; Takahashi, S.; Ishii, T.; Igarashi, K.; Katoh, Y.; Oyake, T.; Hayashi, N.; Satoh, K.; Hatayama, I.; et al. An Nrf2/small Maf heterodimer mediates the induction of phase II detoxifying enzyme genes through antioxidant response elements. *Biochem Biophys Res Commun* **1997**, *236*, 313-322, doi:10.1006/bbrc.1997.6943.
11. Taguchi, K.; Takaku, M.; Egner, P.A.; Morita, M.; Kaneko, T.; Mashimo, T.; Kensler, T.W.; Yamamoto, M. Generation of a New Model Rat: Nrf2 Knockout Rats Are Sensitive to Aflatoxin B1 Toxicity. *Toxicol Sci* **2016**, *152*, 40-52, doi:10.1093/toxsci/kfw065.
12. Mukaigasa, K.; Nguyen, L.T.; Li, L.; Nakajima, H.; Yamamoto, M.; Kobayashi, M. Genetic evidence of an evolutionarily conserved role for Nrf2 in the protection against oxidative stress. *Mol Cell Biol* **2012**, *32*, 4455-4461, doi:10.1128/MCB.00481-12.
13. Xu, P.; Jiang, L.; Yang, Y.; Wu, M.; Liu, B.; Shi, Y.; Shen, Q.; Jiang, X.; He, Y.; Cheng, D.; et al. PAQR4 promotes chemoresistance in non-small cell lung cancer through inhibiting Nrf2 protein degradation. *Theranostics* **2020**, *10*, 3767-3778, doi:10.7150/thno.43142.
14. Schmidt, A.; von Woedtke, T.; Vollmar, B.; Hasse, S.; Bekeschus, S. Nrf2 signaling and inflammation are key events in physical plasma-spurred wound healing. *Theranostics* **2019**, *9*, 1066-1084, doi:10.7150/thno.29754.
15. Zheng, Y.H.; Yang, J.J.; Tang, P.J.; Zhu, Y.; Chen, Z.; She, C.; Chen, G.; Cao, P.; Xu, X.Y. A novel Keap1 inhibitor iKeap1 activates Nrf2 signaling and ameliorates hydrogen peroxide-induced oxidative injury and apoptosis in osteoblasts. *Cell Death Dis* **2021**, *12*, 679, doi:10.1038/s41419-021-03962-8.
16. Keum, Y.S.; Choi, B.Y. Molecular and chemical regulation of the Keap1-Nrf2 signaling

pathway. *Molecules* **2014**, *19*, 10074-10089, doi:10.3390/molecules190710074.
17. Schmidlin, C.J.; Dodson, M.B.; Madhavan, L.; Zhang, D.D. Redox regulation by NRF2 in aging and disease. *Free Radic Biol Med* **2019**, *134*, 702-707, doi:10.1016/j.freeradbiomed.2019.01.016.
18. Wang, M.; Ren, Y.; Hu, S.; Liu, K.; Qiu, L.; Zhang, Y. TCF11 Has a Potent Tumor-Repressing Effect Than Its Prototypic Nrf1alpha by Definition of Both Similar Yet Different Regulatory Profiles, With a Striking Disparity From Nrf2. *Front Oncol* **2021**, *11*, 707032, doi:10.3389/fonc.2021.707032.
19. Ren, Y.; Qiu, L.; Lu, F.; Ru, X.; Li, S.; Xiang, Y.; Yu, S.; Zhang, Y. TALENs-directed knockout of the full-length transcription factor Nrf1alpha that represses malignant behaviour of human hepatocellular carcinoma (HepG2) cells. *Sci Rep* **2016**, *6*, 23775, doi:10.1038/srep23775.
20. Bae, S.H.; Sung, S.H.; Oh, S.Y.; Lim, J.M.; Lee, S.K.; Park, Y.N.; Lee, H.E.; Kang, D.; Rhee, S.G. Sestrins activate Nrf2 by promoting p62-dependent autophagic degradation of Keap1 and prevent oxidative liver damage. *Cell Metab* **2013**, *17*, 73-84, doi:10.1016/j.cmet.2012.12.002.
21. Park, J.S.; Lee, D.H.; Lee, Y.S.; Oh, E.; Bae, K.H.; Oh, K.J.; Kim, H.; Bae, S.H. Dual roles of ULK1 (unc-51 like autophagy activating kinase 1) in cytoprotection against lipotoxicity. *Autophagy* **2020**, *16*, 86-105, doi:10.1080/15548627.2019.1598751.
22. Ito, A.; Shimazu, T.; Maeda, S.; Shah, A.A.; Tsunoda, T.; Iemura, S.; Natsume, T.; Suzuki, T.; Motohashi, H.; Yamamoto, M.; et al. The subcellular localization and activity of cortactin is regulated by acetylation and interaction with Keap1. *Sci Signal* **2015**, *8*, ra120, doi:10.1126/scisignal.aad0667.
23. Audic, S.; Claverie, J.M. The significance of digital gene expression profiles. *Genome Res* **1997**, *7*, 986-995, doi:10.1101/gr.7.10.986.
24. Dong, Z.; Cmarik, J.L. Harvesting cells under anchorage-independent cell transformation conditions for biochemical analyses. *Sci STKE* **2002**, *2002*, pl7, doi:10.1126/stke.2002.130.pl7.
25. Wang, X.Q.; Zhang, W.; Lui, E.L.; Zhu, Y.; Lu, P.; Yu, X.; Sun, J.; Yang, S.; Poon, R.T.; Fan, S.T. Notch1-Snail1-E-cadherin pathway in metastatic hepatocellular carcinoma. *Int J Cancer* **2012**, *131*, E163-172, doi:10.1002/ijc.27336.
26. Villarejo, A.; Cortes-Cabrera, A.; Molina-Ortiz, P.; Portillo, F.; Cano, A. Differential role of Snail1 and Snail2 zinc fingers in E-cadherin repression and epithelial to mesenchymal transition. *J Biol Chem* **2014**, *289*, 930-941, doi:10.1074/jbc.M113.528026.
27. Li, L.; Kobayashi, M.; Kaneko, H.; Nakajima-Takagi, Y.; Nakayama, Y.; Yamamoto, M. Molecular evolution of Keap1. Two Keap1 molecules with distinctive intervening region structures are conserved among fish. *J Biol Chem* **2008**, *283*, 3248-3255, doi:10.1074/jbc.M708702200.
28. Jaramillo, M.C.; Zhang, D.D. The emerging role of the Nrf2-Keap1 signaling pathway in cancer. *Genes Dev* **2013**, *27*, 2179-2191, doi:10.1101/gad.225680.113.
29. Mohs, A.; Otto, T.; Schneider, K.M.; Peltzer, M.; Boekschoten, M.; Holland, C.H.; Hudert, C.A.; Kalveram, L.; Wiegand, S.; Saez-Rodriguez, J.; et al. Hepatocyte-specific NRF2 activation controls fibrogenesis and carcinogenesis in steatohepatitis. *J Hepatol* **2021**, *74*, 638-648, doi:10.1016/j.jhep.2020.09.037.

30. Schulze, K.; Imbeaud, S.; Letouze, E.; Alexandrov, L.B.; Calderaro, J.; Rebouissou, S.; Couchy, G.; Meiller, C.; Shinde, J.; Soysouvanh, F.; et al. Exome sequencing of hepatocellular carcinomas identifies new mutational signatures and potential therapeutic targets. *Nat Genet* **2015**, *47*, 505-511, doi:10.1038/ng.3252.
31. Chaffer, C.L.; Weinberg, R.A. A perspective on cancer cell metastasis. *Science* **2011**, *331*, 1559-1564, doi:10.1126/science.1203543.
32. Ogunwobi, O.O.; Puszyk, W.; Dong, H.J.; Liu, C. Epigenetic upregulation of HGF and c-Met drives metastasis in hepatocellular carcinoma. *PLoS One* **2013**, *8*, e63765, doi:10.1371/journal.pone.0063765.
33. Birchmeier, C.; Birchmeier, W.; Gherardi, E.; Vande Woude, G.F. Met, metastasis, motility and more. *Nat Rev Mol Cell Biol* **2003**, *4*, 915-925, doi:10.1038/nrm1261.
34. Cao, X.; Zhang, Y.; Zhou, Q.; Sun, S.; He, M.; Wang, X.; Ma, P.; Yang, X.; Lv, L.; Zhan, L. Establishment of a Novel Mouse Hepatocellular Carcinoma Model for Dynamic Monitoring of Tumor Development by Bioluminescence Imaging. *Front Oncol* **2022**, *12*, 794101, doi:10.3389/fonc.2022.794101.
35. Chen, J.; Chen, J.; Huang, J.; Li, Z.; Gong, Y.; Zou, B.; Liu, X.; Ding, L.; Li, P.; Zhu, Z.; et al. HIF-2alpha upregulation mediated by hypoxia promotes NAFLD-HCC progression by activating lipid synthesis via the PI3K-AKT-mTOR pathway. *Aging (Albany NY)* **2019**, *11*, 10839-10860, doi:10.18632/aging.102488.
36. Iershov, A.; Nemazanyy, I.; Alkhoury, C.; Girard, M.; Barth, E.; Cagnard, N.; Montagner, A.; Chretien, D.; Rugarli, E.I.; Guillou, H.; et al. The class 3 PI3K coordinates autophagy and mitochondrial lipid catabolism by controlling nuclear receptor PPARalpha. *Nat Commun* **2019**, *10*, 1566, doi:10.1038/s41467-019-09598-9.
37. Wang, Y.; Miao, X.; Jiang, Y.; Wu, Z.; Zhu, X.; Liu, H.; Wu, X.; Cai, J.; Ding, X.; Gong, W. The synergistic antitumor effect of IL-6 neutralization with NVP-BEZ235 in hepatocellular carcinoma. *Cell Death Dis* **2022**, *13*, 146, doi:10.1038/s41419-022-04583-5.
38. Wen, W.; Han, T.; Chen, C.; Huang, L.; Sun, W.; Wang, X.; Chen, S.Z.; Xiang, D.M.; Tang, L.; Cao, D.; et al. Cyclin G1 expands liver tumor-initiating cells by Sox2 induction via Akt/mTOR signaling. *Mol Cancer Ther* **2013**, *12*, 1796-1804, doi:10.1158/1535-7163.MCT-13-0099.